International Journal of Non–Linear Mechanics 185 (2026) 105336

Contents lists available at ScienceDirect

International Journal of Non-Linear Mechanics

journal homepage: www.elsevier.com/locate/nlm

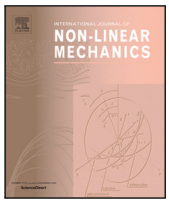

Geometric nonlinear mechanical behavior of anisotropic materials as Cosserat continua

Farui Shi [a,b], Nicholas Fantuzzi [c,*], Minghui Li [a,b], Heping Xie [a,b]

[a] State Key Laboratory of Intelligent Construction and Healthy Operation and Maintenance of Deep Underground Engineering, College of Civil and Transportation Engineering, Shenzhen University, Shenzhen, 518060, China
[b] Guangdong Provincial Key Laboratory of Deep Earth Sciences and Geothermal Energy Exploitation and Utilization, Institute of Deep Earth Sciences and Green Energy, Shenzhen University, Shenzhen, 518060, China
[c] DICAM Department, University of Bologna, Bologna, 40136, Italy

ARTICLE INFO

Keywords:
Geometrical nonlinear behavior
Cosserat theory
Total lagrangian formulation
Anisotropic composite
Scale effect

ABSTRACT

The non-local effect related to microstructures has become increasingly significant in materials like lightweight concrete and honeycombs. Most of such composite materials and structures result in having a nonlinear behavior under applied loads, necessitating advanced computational methods. This study investigates the geometrically nonlinear behavior of anisotropic microstructured materials using a total Lagrangian finite element formulation for the Cosserat continuum. Equivalent anisotropic properties are derived by homogenizing composites featuring different hexagonal microstructural geometries. By analyzing a 2D cantilever beam problem, the nonlinear Cosserat model is compared against the Cauchy continuum and linear versions. Results demonstrate that geometric nonlinear models provide a more realistic description of mechanical responses, particularly under large deformations where linear models prove inadequate. A significant micropolar scale effect is identified on the geometric nonlinear behavior: while Cosserat and Cauchy models converge at small scales, they diverge as the microstructure scale increases relative to the macro scale. Furthermore, different anisotropic configurations exhibit unique load–displacement characteristics, ranging from slightly to highly nonlinear. Although the Cosserat implementation requires higher computational effort than the Cauchy model, this work highlights its value in accurately capturing the non-local features and scale effects inherent in the geometric nonlinear behavior of microstructured composites.

1. Introduction

Composite materials with microstructures such as foams, lightweight concrete, particle assemblies, honeycomb materials, etc., show an increasing application prospect nowadays. For such materials characterized by microstructure that has a non-negligible scale with respect to the macro material scale, the non-local effect becomes important [1,2]. Scale effect on the mechanical behaviors of material has been found experimentally in some previous works [3–7]. In the aspect of computational mechanics, compared to the time-consuming discrete element models, it is known that homogenizing materials as an equivalent continuum can be a fast way to provide satisfactory results for the behavior of microstructured materials [8–10]. When combined with numerical approaches such as the finite element method (FEM), the mechanical analysis of composite materials can achieve higher computational efficiency [11]. However, the classical Cauchy continuum may fail to describe the material behavior sufficiently [12,13], especially for anisotropic materials with microstructures comparable to the material scale. Moreover, when facing nonlinear problems such as large deformation, the disadvantages of the Cauchy continuum would be enlarged, and this continuum would have fewer further applications. This necessitates the application of an alternative continuum that can provide non-local features to inherently bridge micro and macro scales.

The non-local continuum can be defined because the governing equations include parameters revealing the presence of microstructure which can affect the macroscopic behavior [14]. It is known that the Cosserat continuum is a widely used non-local continuum because this continuum introduces additional microrotation and its gradient for each particle, resulting in the characteristic length scale being embedded into the constitutive relation of the Cosserat [15]. The introduction of this continuum theory can be traced back to 1909 [16]. After that, various contributions to extend this theory have been developed [15,17,18]. In the Cosserat continuum, each material point is introduced to a rigid microstructure that can rotate independently from the neighboring medium, bringing a rotation field in addition to

* Corresponding author.
E-mail address: nicholas.fantuzzi@unibo.it (N. Fantuzzi).

https://doi.org/10.1016/j.ijnonlinmec.2026.105336
Received 12 December 2025; Received in revised form 27 January 2026; Accepted 4 February 2026
Available online 12 February 2026

the traditional displacement field. This theory has been demonstrated to be a multi-scale tool to capture the length-scale effects due to the additional kinematic field [19–21]. In the application of finite element implementations, there are a number of references considering linear Cosserat theory on different fields [1,22–28]. Forest and Sab [29] modeled the behavior of heterogeneous materials with linear Cosserat theory. They found that using the Cosserat model, the actual situation can be more precisely approached compared with the Cauchy model. Fractured rock and fiber-reinforced materials can also be satisfactorily studied by this continuum [30–32]. Furthermore, the application of the Cosserat continuum on fluids can also be found [33]. Bhattacharyya and Mukhopadhyay [34] made some updates to the linear Cosserat plate theory. Leonetti et al. [35] investigated the scale effect of microstructures in orthotropic materials and found that the micropolar effect is more apparent as the scale of microstructures is closer to that of the materials. However, the linear Cosserat model cannot always describe the realistic response of microstructured materials.

As for the non-linear aspect, there are a few numerical implementations for the Cosserat model. Basically, the nonlinear simulation of this model is more difficult compared with the classical model. In the Cosserat model, the newly introduced rotation field belongs to the Lie group tensor, which can bring certain difficulties in nonlinear analysis, because such a field is non-additive and non-commutative. This requires more complex mathematical treatments for the rotation field in nonlinear analysis (e.g., when updating the rotation field) [36]. Also, due to the independent rotation field, an additional strain measure should be considered for the Cosserat model compared to just one measure in the Cauchy model. In addition, when considering the geometric nonlinear situations where the deformed and undeformed configurations of material exhibit obvious differences that cannot be neglected as in the linear analysis, it is needed to express measures with respect to a specific configuration. Normally, the Lagrangian formulation is used for solid and structure analysis because it is able to express measures in a known configuration. As a preparation for the nonlinear implementation of the Cosserat model, Pietraszkiewicza and Eremeyev [37,38] reviewed different definitions of strain measures in the Cosserat model and found some measures more suitable to describe the nonlinear Cosserat continuum. Further, Eremeyev and Pietraszkiewicz [39,40] developed a rigorous theoretical framework for the material symmetry group of non-linear polar-elastic continua, extending the theory to include various classes such as orthotropy and transverse isotropy. Using an Updated Lagrangian formulation, Bauer et al. [41] investigated geometrical nonlinear behavior for three-dimensional Cosserat elasticity. Erdelj et al. [42] also studied the geometrical nonlinearity by a detailed formulation and gave results of a set of benchmark problems for the nonlinear Cosserat model. Recently, Misra et al. [43] studied the geometrically nonlinear Cosserat continuum by granular micromechanics. Although consideration of the geometrical nonlinear Cosserat theory can also be referred to by various authors [36,44–48], studies on this topic are still insufficient. Especially, most of the above literature usually limited their study to isotropic materials, whereas anisotropic materials (e.g., anisotropic composite) are rarely investigated.

In this study, we aim to investigate the geometrically nonlinear behavior of anisotropic composites as a Cosserat continuum. The total Lagrangian formulation of this continuum is developed for nonlinear analysis. For comparison, the formulation for the Cauchy continuum is also presented. Composite assumed to be made of hexagonal particles and elastic interfaces can be homogenized as an equivalent Cosserat continuum. By this procedure, different anisotropic material properties can be obtained by adopting three geometries of hexagonal particles termed regular, hourglass, and skew. Since here we are only studying the geometrically nonlinear case, each material property is constant during a specific analysis. The scale effect of microstructures is investigated by changing the scales of the particles. Using the nonlinear finite element method, the simulations are performed on a planar cantilever beam problem under a load with constant direction at its free end, which is able to show clear geometric nonlinearity under larger deformation.

This work is structured as follows. After the introduction section, the total Lagrangian formulation for geometric nonlinear Cauchy and Cosserat continua is illustrated in Section 2. In Section 3, Numerical simulations and anisotropic material properties are presented. Section 4 shows the numerical results and related discussions. Finally, some conclusions and remarks are drawn in Section 5.

2. Geometric nonlinear finite element formulations

In the linear analysis, the deformation of the continuum is assumed to be infinitesimal and thus the difference between the undeformed and deformed configuration can be neglected. Linear Cosserat finite element formulation can be found in much early literature [49–51]. However, the assumption of linearity may be neither appropriate nor realistic to describe a real material response, such as larger deformation. This motivates the study on nonlinear analysis. Here we focus on the so-called geometric nonlinear analysis where the deformation is no longer infinitesimal and we should distinguish between the undeformed and deformed configurations. The basic problem in a general nonlinear analysis is to find the state of equilibrium of a body corresponding to the applied loads [52]:

$$^{j+1}\mathbf{r} = {}^{j+1}\mathbf{f} \tag{1}$$

where $^{j+1}\mathbf{r}$ and $^{j+1}\mathbf{f}$ are external and internal force vectors at deformed configuration $j+1$. $^{j+1}\mathbf{f}$ can be linearized as:

$$^{j+1}\mathbf{f} = {}^{j}\mathbf{f} + \Delta\mathbf{f} \tag{2}$$

where $^{j}\mathbf{f}$ is internal force vectors stored at last configuration j. $\Delta\mathbf{f}$ is the increment internal force vectors corresponding to the increment displacement. This vector can be approximated as:

$$\Delta\mathbf{f} = \mathbf{K}\Delta\mathbf{d} \tag{3}$$

where $\mathbf{K}$ is the tangent stiffness matrix and $\Delta\mathbf{d}$ is the increment displacement. Substituting Eqs. (2) and (3) into Eq. (1), we have:

$$\mathbf{K}\Delta\mathbf{d} = {}^{j+1}\mathbf{r} - {}^{j}\mathbf{f} = \Delta\mathbf{f} \tag{4}$$

The formulation of a nonlinear finite element method is normally performed as a sequence of loading or time steps t. For each step, an increment external loading is applied and Eq. (4) needs to be solved by some iteration steps k (Newton–Raphson method). In the following, based on Eq. (4), the total Lagrangian finite element formulations will be performed on the classical Cauchy continuum and Cosserat continuum to study the geometric nonlinear problems. In the total Lagrangian formulation, all measures refer to the initial or undeformed configuration. We suppose that we are in the tth load step and the solution for the kth iteration step has been found but the convergence criterion has not yet been satisfied, thus we should solve the problem for the $(k+1)$th iteration step. After getting the solution at $(k+1)$th iteration step, we need to update relative measures in this step and continue the iteration procedure until the convergence criterion is satisfied.

2.1. Geometric nonlinear Cauchy continuum

In the geometric nonlinear analysis, since considering the deformed (current) configuration differs from the undeformed (reference) configuration, measures such as stress and strain are unknown in the deformed configuration. Thus, measures expressed with respect to the known undeformed configuration should be introduced. Here, we focus on the two-dimensional (2D) problems. The energetically conjugated stress and strain measures that we shall use in the Cauchy continuum

are the second Piola–Kirchhoff stress tensor $\mathbf{S}$ and the Green–Lagrange strain tensor $\mathbf{E}$:

$$\begin{aligned}\mathbf{S} &= J\mathbf{F}^{-1}\cdot\boldsymbol{\sigma}\cdot\mathbf{F}^{-\top}\\ \mathbf{E} &= \tfrac{1}{2}(\mathbf{F}^{\top}\cdot\mathbf{F}-\mathbf{I}) = \tfrac{1}{2}[\nabla_0\mathbf{u}+(\nabla_0\mathbf{u})^{\top}+(\nabla_0\mathbf{u})\cdot(\nabla_0\mathbf{u})^{\top}]\end{aligned} \tag{5}$$

where $\boldsymbol{\sigma}$ is the Cauchy or true stress tensor in a deformed configuration. $\mathbf{u} = \begin{bmatrix}u_1 & u_2\end{bmatrix}^{\top}$ is the displacement vector and ∇_0 is the gradient operator with respect to the reference configuration. $\mathbf{F}$ means the deformation gradient, $\mathbf{F} = \frac{\partial \mathbf{x}}{\partial \mathbf{X}}$, where $\mathbf{x}$ denotes a spatial position vector of a continuum particle in the current configuration, and $\mathbf{X}$ represents a material position vector of this particle in the reference configuration. $\mathbf{F}$ in the 2D matrix form as:

$$\mathbf{F} = \begin{bmatrix}\frac{\partial x_1}{\partial X_1} & \frac{\partial x_1}{\partial X_2}\\ \frac{\partial x_2}{\partial X_1} & \frac{\partial x_2}{\partial X_2}\end{bmatrix} \tag{6}$$

or,

$$\mathbf{F} = \nabla_0\mathbf{u}+\mathbf{I} = \begin{bmatrix}\frac{\partial u_1}{\partial X_1} & \frac{\partial u_1}{\partial X_2}\\ \frac{\partial u_2}{\partial X_1} & \frac{\partial u_2}{\partial X_2}\end{bmatrix} + \begin{bmatrix}1 & 0\\ 0 & 1\end{bmatrix} \tag{7}$$

since $\mathbf{x} = \mathbf{X}+\mathbf{u}$. The determinant of $\mathbf{F}$ can be defined as:

$$J = \det(\mathbf{F}) > 0 \tag{8}$$

The total Lagrangian formulation has been well-established for the Cauchy continuum [52,53]. Firstly, the weak form of the virtual work in terms of undeformed configuration can be expressed as:

$$\int_V \delta\mathbf{E} : \mathbf{S}\mathrm{d}V = \int_V \delta\mathbf{u}^{\top}\mathbf{b}\mathrm{d}V + \int_S \delta\mathbf{u}^{\top}\mathbf{t}\mathrm{d}S \tag{9}$$

where δ is the variational operator, $\mathbf{b}$ is the body force vector. $\mathbf{t}$ is the traction applied on the surface boundary S.

$\mathbf{S}$ and $\mathbf{E}$ can be decomposed as:

$$\begin{aligned}\mathbf{S} &= \mathbf{S}^t + \boldsymbol{s}\\ \mathbf{E} &= \mathbf{E}^t + \boldsymbol{\varepsilon} = \boldsymbol{\varepsilon}\\ \boldsymbol{\varepsilon} &= \boldsymbol{e}+\boldsymbol{\eta}\end{aligned} \tag{10}$$

where $\mathbf{S}^t$ and $\mathbf{E}^t$ are the known stress and strain at tth load step. $\boldsymbol{s}$ and $\boldsymbol{\varepsilon}$ are increment stress and strain. $\boldsymbol{e}$ and $\boldsymbol{\eta}$ are the linear and nonlinear part of $\boldsymbol{\varepsilon}$:

$$\begin{aligned}e_{ij} &= \frac{1}{2}\left(\frac{\partial u_i}{\partial X_j}+\frac{\partial u_j}{\partial X_i}+\frac{\partial u_k^t}{\partial X_i}\frac{\partial u_k}{\partial X_j}+\frac{\partial u_k^t}{\partial X_j}\frac{\partial u_k}{\partial X_i}\right)\\ \eta_{ij} &= \frac{1}{2}\frac{\partial u_k}{\partial X_i}\frac{\partial u_k}{\partial X_j}\end{aligned} \tag{11}$$

Considering Eq. (10) and a constant material constitutive matrix $\mathbf{C}$, after some algebra and linearization processes, the weak form of the virtual work becomes:

$$\begin{aligned}\int_V \delta\boldsymbol{e} : (\mathbf{C} : \boldsymbol{e})\mathrm{d}V + \int_V \delta\boldsymbol{\eta} : \mathbf{S}^t\mathrm{d}V = \\ \left(\int_V \delta\mathbf{u}^{\top}\mathbf{b}\mathrm{d}V + \int_S \delta\mathbf{u}^{\top}\mathbf{t}\mathrm{d}S\right) - \int_V \delta\boldsymbol{e} : \mathbf{S}^t\mathrm{d}V\end{aligned} \tag{12}$$

Now considering the approximation of the displacement field by nodal displacement values in a element:

$$\mathbf{u} = \mathbf{N}\boldsymbol{d}^e \tag{13}$$

where $\mathbf{N}$ is the shape function. $\boldsymbol{d}^e = [u_1^1\ u_1^2\ \cdots\ u_1^n\ u_2^1\ u_2^2\ \cdots\ u_2^n]^{\top}$ is the nodal displacement in a element. n is the node number. Eq. (13) in matrix form as:

$$\begin{bmatrix}u_1\\ u_2\end{bmatrix} = \begin{bmatrix}N_1 & N_2 & \cdots & N_n & 0 & 0 & \cdots & 0\\ 0 & 0 & \cdots & 0 & N_1 & N_2 & \cdots & N_n\end{bmatrix}\begin{bmatrix}u_1^1\\ u_1^2\\ \cdots\\ u_1^n\\ u_2^1\\ u_2^2\\ \cdots\\ u_2^n\end{bmatrix} \tag{14}$$

Substituting Eq. (13) into Eq. (12), we can obtain:

$$\begin{aligned}\delta\boldsymbol{d}^e\int_V(\mathbf{B_L})^{\top}\mathbf{C}(\mathbf{B_L})\boldsymbol{d}^e\mathrm{d}V + \delta\boldsymbol{d}^e\int_V(\mathbf{B_{NL}})^{\top}\mathbf{S}^t(\mathbf{B_{NL}})\boldsymbol{d}^e\mathrm{d}V = \\ \left(\delta\boldsymbol{d}^e\int_V\mathbf{N}^{\top}\mathbf{b}\mathrm{d}V + \delta\boldsymbol{d}^e\int_S\mathbf{N}^{\top}\mathbf{t}\mathrm{d}S\right) - \delta\boldsymbol{d}^e\int_V(\mathbf{B_L})^{\top}\mathbf{S}_v^t\mathrm{d}V\end{aligned} \tag{15}$$

For arbitrary $\delta\boldsymbol{d}^e$, above equation becomes:

$$\begin{aligned}&\left(\int_V(\mathbf{B_L})^{\top}\mathbf{C}(\mathbf{B_L})\mathrm{d}V + \int_V(\mathbf{B_{NL}})^{\top}\mathbf{S}^t(\mathbf{B_{NL}})\mathrm{d}V\right)\boldsymbol{d}^e\\ &= \left(\int_V\mathbf{N}^{\top}\mathbf{b}\mathrm{d}V + \int_S\mathbf{N}^{\top}\mathbf{t}\mathrm{d}S\right) - \int_V(\mathbf{B_L})^{\top}\mathbf{S}_v^t\mathrm{d}V\end{aligned} \tag{16}$$

where the measures in Eq. (16) are arranged as follows:

$$\begin{aligned}\mathbf{b} &= \begin{bmatrix}b_1\\ b_2\end{bmatrix},\quad \mathbf{t} = \begin{bmatrix}t_1\\ t_2\end{bmatrix}\\ \mathbf{C} &= \begin{bmatrix}C_{1111} & C_{1122} & C_{1112}\\ C_{2211} & C_{2222} & C_{2212}\\ C_{1211} & C_{1222} & C_{1212}\end{bmatrix}\\ \mathbf{S}^t &= \begin{bmatrix}S_{11}^t & S_{12}^t & 0 & 0\\ S_{12}^t & S_{22}^t & 0 & 0\\ 0 & 0 & S_{11}^t & S_{12}^t\\ 0 & 0 & S_{12}^t & S_{22}^t\end{bmatrix}\\ \mathbf{S}_v^t &= \begin{bmatrix}S_{11}^t\\ S_{22}^t\\ S_{12}^t\end{bmatrix} = \begin{bmatrix}C_{1111} & C_{1122} & C_{1112}\\ C_{2211} & C_{2222} & C_{2212}\\ C_{1211} & C_{1222} & C_{1212}\end{bmatrix}\begin{bmatrix}E_{11}\\ E_{22}\\ 2E_{12}\end{bmatrix}\end{aligned} \tag{17}$$

$\mathbf{B_L} = \mathbf{B_L^0} + \mathbf{B_L^u} + \mathbf{B_L^v}$, where (see the equation in Box I), If let,

$$\begin{aligned}\mathbf{K_L^e} &= \int_V(\mathbf{B_L})^{\top}\mathbf{C}(\mathbf{B_L})\mathrm{d}V\\ \mathbf{K_{NL}^e} &= \int_V(\mathbf{B_{NL}})^{\top}\mathbf{S}^t(\mathbf{B_{NL}})\mathrm{d}V\\ \mathbf{r^e} &= \int_V\mathbf{N}^{\top}\mathbf{b}\mathrm{d}V + \int_S\mathbf{N}^{\top}\mathbf{t}\mathrm{d}S\\ \mathbf{f^e} &= \int_V(\mathbf{B_L})^{\top}\mathbf{S}_v^t\mathrm{d}V\end{aligned} \tag{19}$$

so Eq. (16) becomes:

$$\left(\mathbf{K_L^e}+\mathbf{K_{NL}^e}\right)\mathbf{d^e} = \mathbf{r^e}-\mathbf{f^e} \tag{20}$$

$$\mathbf{K^e}\mathbf{d^e} = \mathbf{r^e}-\mathbf{f^e} \tag{21}$$

Thus, we have the same form as Eq. (4) at the element level. By assembling all element contributions to a global form through a standard finite element procedure, we can get the solution of the global increment displacement vector $\boldsymbol{\Delta}\mathbf{d}$ for an iteration step. Next, we can update measures such as total displacement, strain, and stress for the next iteration step and then move to the calculation of the next iteration. Considering a superscript representing the iteration step, the displacement and node coordinates can be updated as:

$$\begin{aligned}\mathbf{u}^{(k+1)} &= \mathbf{u}^{(k)}+\boldsymbol{\Delta}\mathbf{d}\\ \mathbf{x}^{(k+1)} &= \mathbf{x}^{(k)}+\boldsymbol{\Delta}\mathbf{d}\end{aligned} \tag{22}$$

2.2. Geometric nonlinear Cosserat continuum

In the 2D Cosserat continuum, an extra degree of freedom (micro-rotation φ) is introduced for each material particle in addition to two classical translation degrees of freedom (u_1, u_2). As the introduction of φ, the kinematic equation of this continuum should involve so-called curvature measures (χ_1, χ_2) and the classical strain measures become non-symmetric, i.e $\varepsilon_{12} \neq \varepsilon_{21}$. Consequently, there are two additional couple stress measures μ_1, μ_2 and the classical stress measures also become non-symmetric ($\sigma_{12} \neq \sigma_{21}$). Linear anisotropic stress–strain

$$
\mathbf{B}_{\mathbf{L}}^{\mathbf{0}} = \begin{bmatrix} \frac{\partial N_1}{\partial X_1} & \frac{\partial N_2}{\partial X_1} & \cdots & \frac{\partial N_n}{\partial X_1} & 0 & 0 & \cdots & 0 \\ 0 & 0 & \cdots & 0 & \frac{\partial N_1}{\partial X_2} & \frac{\partial N_2}{\partial X_2} & \cdots & \frac{\partial N_n}{\partial X_2} \\ \frac{\partial N_1}{\partial X_2} & \frac{\partial N_2}{\partial X_2} & \cdots & \frac{\partial N_n}{\partial X_2} & \frac{\partial N_1}{\partial X_1} & \frac{\partial N_2}{\partial X_1} & \cdots & \frac{\partial N_n}{\partial X_1} \end{bmatrix}
$$

$$
\mathbf{B}_{\mathbf{L}}^{\mathbf{u}} = \begin{bmatrix} \frac{\partial u_1}{\partial X_1}\frac{\partial N_1}{\partial X_1} & \frac{\partial u_1}{\partial X_1}\frac{\partial N_2}{\partial X_1} & \cdots & \frac{\partial u_1}{\partial X_1}\frac{\partial N_n}{\partial X_1} & 0 & 0 & \cdots & 0 \\ \frac{\partial u_1}{\partial X_2}\frac{\partial N_1}{\partial X_2} & \frac{\partial u_1}{\partial X_2}\frac{\partial N_2}{\partial X_2} & \cdots & \frac{\partial u_1}{\partial X_2}\frac{\partial N_n}{\partial X_2} & 0 & 0 & \cdots & 0 \\ \frac{\partial u_1}{\partial X_1}\frac{\partial N_1}{\partial X_2} + \frac{\partial u_1}{\partial X_2}\frac{\partial N_1}{\partial X_1} & \frac{\partial u_1}{\partial X_1}\frac{\partial N_2}{\partial X_2} + \frac{\partial u_1}{\partial X_2}\frac{\partial N_2}{\partial X_1} & \cdots & \frac{\partial u_1}{\partial X_1}\frac{\partial N_n}{\partial X_2} + \frac{\partial u_1}{\partial X_2}\frac{\partial N_n}{\partial X_1} & 0 & 0 & \cdots & 0 \end{bmatrix}
$$

$$
\mathbf{B}_{\mathbf{L}}^{\mathbf{v}} = \begin{bmatrix} 0 & 0 & \cdots & 0 & \frac{\partial u_2}{\partial X_1}\frac{\partial N_1}{\partial X_1} & \frac{\partial u_2}{\partial X_1}\frac{\partial N_2}{\partial X_1} & \cdots & \frac{\partial u_2}{\partial X_1}\frac{\partial N_n}{\partial X_1} \\ 0 & 0 & \cdots & 0 & \frac{\partial u_2}{\partial X_2}\frac{\partial N_1}{\partial X_2} & \frac{\partial u_2}{\partial X_2}\frac{\partial N_2}{\partial X_2} & \cdots & \frac{\partial u_2}{\partial X_2}\frac{\partial N_n}{\partial X_2} \\ 0 & 0 & \cdots & 0 & \frac{\partial u_2}{\partial X_1}\frac{\partial N_1}{\partial X_2} + \frac{\partial u_2}{\partial X_2}\frac{\partial N_1}{\partial X_1} & \frac{\partial u_2}{\partial X_1}\frac{\partial N_2}{\partial X_2} + \frac{\partial u_2}{\partial X_2}\frac{\partial N_2}{\partial X_1} & \cdots & \frac{\partial u_2}{\partial X_1}\frac{\partial N_n}{\partial X_2} + \frac{\partial u_2}{\partial X_2}\frac{\partial N_n}{\partial X_1} \end{bmatrix}
$$

$$
\mathbf{B}_{\mathbf{NL}} = \begin{bmatrix} \frac{\partial N_1}{\partial x_1} & \frac{\partial N_2}{\partial x_1} & \cdots & \frac{\partial N_n}{\partial x_1} & 0 & 0 & \cdots & 0 \\ \frac{\partial N_1}{\partial x_2} & \frac{\partial N_2}{\partial x_2} & \cdots & \frac{\partial N_n}{\partial x_2} & 0 & 0 & \cdots & 0 \\ 0 & 0 & \cdots & 0 & \frac{\partial N_1}{\partial x_1} & \frac{\partial N_2}{\partial x_1} & \cdots & \frac{\partial N_n}{\partial x_1} \\ 0 & 0 & \cdots & 0 & \frac{\partial N_1}{\partial x_2} & \frac{\partial N_2}{\partial x_2} & \cdots & \frac{\partial N_n}{\partial x_2} \end{bmatrix} \tag{18}
$$

Box I.

relations for the Cosserat model can be written as [54]:

$$
\begin{Bmatrix} \sigma_{11} \\ \sigma_{22} \\ \sigma_{12} \\ \sigma_{21} \\ \mu_1 \\ \mu_2 \end{Bmatrix} = \begin{bmatrix} A_{1111} & A_{1122} & A_{1112} & A_{1121} & B_{111} & B_{112} \\ A_{2211} & A_{2222} & A_{2212} & A_{2221} & B_{221} & B_{222} \\ A_{1211} & A_{1222} & A_{1212} & A_{1221} & B_{121} & B_{122} \\ A_{2111} & A_{2122} & A_{2112} & A_{2121} & B_{211} & B_{212} \\ B_{111} & B_{122} & B_{112} & B_{121} & D_{11} & D_{12} \\ B_{211} & B_{222} & B_{212} & B_{221} & D_{21} & D_{22} \end{bmatrix} \begin{Bmatrix} \varepsilon_{11} \\ \varepsilon_{22} \\ \varepsilon_{12} \\ \varepsilon_{21} \\ \chi_1 \\ \chi_2 \end{Bmatrix} \tag{23}
$$

for hyperelastic materials, $A_{ijhk} = A_{hkij}$, $B_{ijh} = B_{hij}$, $D_{ij} = D_{ji}$ $(i, j, h, k = 1, 2)$. By collecting A_{ijhk}, B_{ijh}, and D_{ij} into the tensors $\mathbb{A}$, $\mathbb{B}$, and $\mathbb{D}$. Eq. (23) has the form of:

$$
\begin{aligned} \boldsymbol{\sigma} &= \mathbb{A} : \boldsymbol{\varepsilon} + \mathbb{B} : \boldsymbol{\chi} \\ \boldsymbol{\mu} &= \mathbb{B}^{\top} : \boldsymbol{\varepsilon} + \mathbb{D} : \boldsymbol{\chi} \end{aligned} \tag{24}
$$

where tensors,

$$
\boldsymbol{\sigma} = \begin{bmatrix} \sigma_{11} & \sigma_{12} \\ \sigma_{21} & \sigma_{22} \end{bmatrix}, \quad \boldsymbol{\mu} = \begin{bmatrix} \mu_1 & \mu_2 \end{bmatrix}
$$
$$
\boldsymbol{\varepsilon} = \begin{bmatrix} \varepsilon_{11} & \varepsilon_{12} \\ \varepsilon_{21} & \varepsilon_{22} \end{bmatrix}, \quad \boldsymbol{\chi} = \begin{bmatrix} \chi_1 & \chi_2 \end{bmatrix} \tag{25}
$$

The above measures are based on the current configuration. However, for the geometric nonlinear analysis, measures based on the reference configurations should be considered as mentioned above. Various strain measures for non-linear analysis have been derived for the micropolar continuum in literature [37]. Here, we select strain and curvature measures as:

$$
\mathbf{E} = \mathbf{Q}^{\top}\mathbf{F} - \mathbf{I} \tag{26}
$$

$$
\mathbf{K} = -\frac{1}{2}\boldsymbol{\epsilon} : (\mathbf{Q}^{\top}\nabla_0\mathbf{Q}) \tag{27}
$$

The derived strain and curvature measures can be referred to as Cosserat Lagrangian strain tensor and the Cosserat Lagrangian curvature tensor. These two measures can be also referred to as stretch tensor and wryness tensor [37] or Biot-like strain tensors [42]. The energetically conjugated Cosserat Lagrangian stress and couple stress measures are:

$$
\mathbf{B} = J\mathbf{Q}^{\top}\boldsymbol{\sigma}\mathbf{F}^{-\top} \tag{28}
$$

$$
\mathbf{G} = J\mathbf{Q}^{\top}\boldsymbol{\mu}\mathbf{F}^{-\top} \tag{29}
$$

Since here we only focus on the geometric non-linear analysis, the material relation shown in Eq. (23) remains unchanged for Cosserat Lagrangian measures, i.e.

$$
\begin{aligned} \mathbf{B} &= \mathbb{A} : \mathbf{E} + \mathbb{B} : \mathbf{K} \\ \mathbf{G} &= \mathbb{B}^{\top} : \mathbf{E} + \mathbb{D} : \mathbf{K} \end{aligned} \tag{30}
$$

where tensors **B**, **G**, **E**, and **K** follow the form as shown in Eq. (25).

In Eqs. (26)–(29), **Q** is the proper orthogonal microrotation tensor which is related to the microrotation vector $\boldsymbol{\phi} = \begin{bmatrix} \phi_1 & \phi_2 & \phi_3 \end{bmatrix}^{\top}$. The magnitude of this vector is $\|\phi\|$ and the skew-symmetric tensor $\hat{\boldsymbol{\phi}}$ corresponding to the microrotation vector can be constructed as:

$$
\hat{\boldsymbol{\phi}} = \begin{bmatrix} 0 & -\phi_3 & \phi_2 \\ \phi_3 & 0 & -\phi_1 \\ -\phi_2 & \phi_1 & 0 \end{bmatrix} \tag{31}
$$

The microrotation tensor **Q** corresponding to $\boldsymbol{\phi}$ can be expressed according to the Euler–Rodrigues formula [46]:

$$
\mathbf{Q}(\boldsymbol{\phi}) = \mathbf{I} + \frac{\sin\|\boldsymbol{\phi}\|}{\|\boldsymbol{\phi}\|}\hat{\boldsymbol{\phi}} + \frac{1 - \cos\|\boldsymbol{\phi}\|}{\|\boldsymbol{\phi}\|^2}\hat{\boldsymbol{\phi}}\hat{\boldsymbol{\phi}} \tag{32}
$$

where **Q** satisfies $\mathbf{Q}^{-1} = \mathbf{Q}^{\top}$ and $\det(\mathbf{Q}) = 1$ since **Q** is an orthogonal tensor.

In 2D case, $\boldsymbol{\phi}$ only includes one component $\phi_3 := \varphi$. Thus, $\hat{\boldsymbol{\phi}}$ and **Q** can be expressed as:

$$
\hat{\boldsymbol{\phi}} = \hat{\varphi} = \begin{bmatrix} 0 & -\varphi \\ \varphi & 0 \end{bmatrix} \tag{33}
$$

$$
\mathbf{Q} = \begin{bmatrix} \cos\varphi & -\sin\varphi \\ \sin\varphi & \cos\varphi \end{bmatrix} \tag{34}
$$

in the rest of this study, we denote an arbitrary quantity with $\hat{}$ as:

$$
\hat{\lambda} = \begin{bmatrix} 0 & -\lambda \\ \lambda & 0 \end{bmatrix} = \lambda \begin{bmatrix} 0 & -1 \\ 1 & 0 \end{bmatrix} = \lambda\hat{\mathbf{I}} \tag{35}
$$

In order to implement the principle of virtual work, virtual Cosserat Lagrangian strain and curvature measures should be derived. At the first, since **Q** is an orthogonal tensor, virtual **Q** can be denoted as $\delta\mathbf{Q} = \delta\hat{\varphi}\mathbf{Q}$ [36]. Then, applying some mathematical manipulations, the virtual Cosserat Lagrangian strain tensor and curvature tensor are given by:

$$
\delta\mathbf{E} = \mathbf{Q}^{\top}(\nabla_0\delta\mathbf{u} + \delta\hat{\varphi}^{\top}\mathbf{F}) \tag{36}
$$

$$
\delta\mathbf{K} = \mathbf{Q}^{\top}\nabla_0\delta\varphi \tag{37}
$$

With the virtual measures of strain and curvature, the virtual work equation is given as:

$$\int_V \left((\delta\mathbf{E})^\top : \mathbf{B}^\top + (\delta\mathbf{K})^\top : \mathbf{G}^\top\right) \mathrm{d}V = \int_V (\delta\mathbf{u}^\top \mathbf{b}_v + \delta\varphi^\top \mathbf{m}_v)\mathrm{d}V + \int_S (\delta\mathbf{u}^\top \mathbf{t}_s + \delta\varphi^\top \mathbf{m}_s)\mathrm{d}S \tag{38}$$

where $\mathbf{b}_v$ and $\mathbf{m}_v$ are body force and body couple force, $\mathbf{t}_s$ and $\mathbf{m}_s$ are traction and couple traction on S.

Next in FEM, adding nodal microrotation into $\boldsymbol{d}^e$, we can have a new vector of element nodal degrees of freedom as:

$$\boldsymbol{d}^e = [u_1^1\ u_1^2\ \cdots\ u_1^n\ u_2^1\ u_2^2\ \cdots\ u_2^n\ \varphi^1\ \varphi^2\ \cdots\ \varphi^n]^\top \tag{39}$$

so the kinematic displacement and microrotation fields can be approximated at the element level as:

$$\begin{bmatrix} u_1 \\ u_2 \\ \varphi \end{bmatrix} = \begin{bmatrix} N_1 & N_2 \cdots N_n & 0 & 0 \cdots 0 & 0 & 0 \cdots 0 \\ 0 & 0 \cdots 0 & N_1 & N_2 \cdots N_n & 0 & 0 \cdots 0 \\ 0 & 0 \cdots 0 & 0 & 0 \cdots 0 & N_1 & N_2 \cdots N_n \end{bmatrix} \begin{bmatrix} u_1^1 \\ u_1^2 \\ \cdots \\ u_1^n \\ u_2^1 \\ u_2^2 \\ \cdots \\ u_2^n \\ \varphi^1 \\ \varphi^2 \\ \cdots \\ \varphi^n \end{bmatrix} \tag{40}$$

we refer to:

$$\begin{aligned} u_1 &= \mathbf{N}_u \boldsymbol{d}^e \\ u_2 &= \mathbf{N}_v \boldsymbol{d}^e \\ \varphi &= \mathbf{N}_\varphi \boldsymbol{d}^e \\ \mathbf{N}_\mathbf{u} &= \begin{bmatrix} \mathbf{N}_u \\ \mathbf{N}_v \end{bmatrix} \end{aligned} \tag{41}$$

Using the approximated kinematic fields, firstly, the virtual external work $\mathcal{R}$ can be obtained as:

$$\mathcal{R} = \delta\boldsymbol{d}^{e\top} \left(\int_V (\mathbf{N}_\mathbf{u}^\top \mathbf{b}_v + \mathbf{N}_\varphi^\top \mathbf{m}_v)\mathrm{d}V + \int_S (\mathbf{N}_\mathbf{u}^\top \mathbf{t}_s + \mathbf{N}_\varphi^\top \mathbf{m}_s)\mathrm{d}S \right) \tag{42}$$

As for the virtual internal work $\mathcal{F}$, the interpolated virtual Cosserat Lagrangian strain tensor and curvature tensor are:

$$\begin{aligned} (\delta\mathbf{E})^\top &= (\mathbf{Q}^\top \nabla_0 \delta\mathbf{u})^\top + (\mathbf{Q}^\top \delta\hat{\varphi}^\top \mathbf{F})^\top \\ &= (\mathbf{Q}^\top (\nabla_0 \mathbf{N}_\mathbf{u}) \delta\mathbf{d}^\mathbf{e})^\top + (\mathbf{Q}^\top \hat{\mathbf{I}}^\top \mathbf{F} \mathbf{N}_\varphi \delta\mathbf{d}^\mathbf{e})^\top \\ &= \delta\boldsymbol{d}^{e\top} (\nabla_0 \mathbf{N}_\mathbf{u})^\top \mathbf{Q} + \delta\boldsymbol{d}^{e\top} \mathbf{N}_\varphi^\top \mathbf{F}^\top \hat{\mathbf{I}} \mathbf{Q} \\ (\delta\mathbf{K})^\top &= (\mathbf{Q}^\top \nabla_0 \delta\varphi)^\top \\ &= (\mathbf{Q}^\top (\nabla_0 \mathbf{N}_\varphi) \delta\mathbf{d}^\mathbf{e})^\top \\ &= \delta\boldsymbol{d}^{e\top} (\nabla_0 \mathbf{N}_\varphi)^\top \mathbf{Q} \end{aligned} \tag{43}$$

where,

$$(\nabla_0 \mathbf{N}_\mathbf{u})^\top = \begin{bmatrix} \frac{\partial \mathbf{N}_u^\top}{\partial \mathrm{X}_1} & \frac{\partial \mathbf{N}_v^\top}{\partial \mathrm{X}_1} \\ \frac{\partial \mathbf{N}_u^\top}{\partial \mathrm{X}_2} & \frac{\partial \mathbf{N}_v^\top}{\partial \mathrm{X}_2} \end{bmatrix}, \quad (\nabla_0 \mathbf{N}_\varphi)^\top = \begin{bmatrix} \frac{\partial \mathbf{N}_\varphi^\top}{\partial \mathrm{X}_1} & \frac{\partial \mathbf{N}_\varphi^\top}{\partial \mathrm{X}_2} \end{bmatrix}$$

As the virtual work $\mathcal{R} = \mathcal{F}$, for arbitrary $\delta\boldsymbol{d}^e$, external $\mathbf{r}$ and internal $\mathbf{f}$ force vectors can be obtained from Eqs. (38), (42) and (43):

$$\mathbf{r} = \int_V (\mathbf{N}_\mathbf{u}^\top \mathbf{b}_v + \mathbf{N}_\varphi^\top \mathbf{m}_v)\mathrm{d}V + \int_S (\mathbf{N}_\mathbf{u}^\top \mathbf{t}_s + \mathbf{N}_\varphi^\top \mathbf{m}_s)\mathrm{d}S \tag{44}$$

$$\mathbf{f} = \int_V \left((\nabla_0 \mathbf{N}_\mathbf{u})^\top \mathbf{Q} : \mathbf{B}^\top + \mathbf{N}_\varphi^\top \mathbf{F}^\top \hat{\mathbf{I}} \mathbf{Q} : \mathbf{B}^\top + (\nabla_0 \mathbf{N}_\varphi)^\top \mathbf{Q} : \mathbf{G}^\top \right) \mathrm{d}V \tag{45}$$

At element level, the ith component of element internal force vector $\mathbf{f}^\mathbf{e}$ can be expressed as:

$$\mathrm{f}_i^\mathbf{e} = \int_V \left((\nabla_0 \mathbf{N}_{\mathbf{u}i})^\top \mathbf{Q} : \mathbf{B}^\top + N_{\varphi i} \mathbf{F}^\top \hat{\mathbf{I}} \mathbf{Q} : \mathbf{B}^\top + (\nabla_0 N_{\varphi i})^\top \mathbf{Q} : \mathbf{G}^\top \right) \mathrm{d}V \tag{46}$$

where,

$$(\nabla_0 \mathbf{N}_{\mathbf{u}i})^\top = \begin{bmatrix} \frac{\partial N_{ui}}{\partial \mathrm{X}_1} & \frac{\partial N_{vi}}{\partial \mathrm{X}_1} \\ \frac{\partial N_{ui}}{\partial \mathrm{X}_2} & \frac{\partial N_{vi}}{\partial \mathrm{X}_2} \end{bmatrix}, \quad (\nabla_0 N_{\varphi i})^\top = \begin{bmatrix} \frac{\partial N_{\varphi i}}{\partial \mathrm{X}_1} & \frac{\partial N_{\varphi i}}{\partial \mathrm{X}_2} \end{bmatrix}$$

In order to get a form as Eq. (4), the incremental internal force vector should be approximated as a linear form. Erdelj et al. [42] presented the increment strain ($\Delta\mathbf{E}$) and curvature ($\Delta\mathbf{K}$) that coincide in their virtual form given in Eqs. (36) and (37) as:

$$\begin{aligned} \Delta\mathbf{E} &= \mathbf{Q}^\top (\nabla_0 \Delta\mathbf{u} + \Delta\hat{\varphi}^\top \mathbf{F}) \\ \Delta\mathbf{K} &= \mathbf{Q}^\top \nabla_0 \Delta\varphi \end{aligned} \tag{47}$$

where,

$$\Delta\mathbf{Q} = \Delta\hat{\varphi}\mathbf{Q}$$

Next, incremental form of each integrand term in $\mathbf{f}_i^e$ (Eq. (46)) is formulated as:

$$\begin{aligned} \Delta\mathrm{f}_i^{\mathbf{e}1} &= (\nabla_0 \mathbf{N}_{\mathbf{u}i})^\top \Delta\mathbf{Q} : \mathbf{B}^\top + (\nabla_0 \mathbf{N}_{\mathbf{u}i})^\top \mathbf{Q} : (\Delta\mathbf{B})^\top \\ \Delta\mathrm{f}_i^{\mathbf{e}2} &= N_{\varphi i} (\nabla_0 \Delta\mathbf{u})^\top \hat{\mathbf{I}} \mathbf{Q} : \mathbf{B}^\top + N_{\varphi i} \mathbf{F}^\top \hat{\mathbf{I}} \Delta\mathbf{Q} : \mathbf{B}^\top + N_{\varphi i} \mathbf{F}^\top \hat{\mathbf{I}} \mathbf{Q} : (\Delta\mathbf{B})^\top \\ \Delta\mathrm{f}_i^{\mathbf{e}3} &= (\nabla_0 N_{\varphi i})^\top \Delta\mathbf{Q} : \mathbf{G}^\top + (\nabla_0 N_{\varphi i})^\top \mathbf{Q} : (\Delta\mathbf{G})^\top \end{aligned} \tag{48}$$

where,

$$\begin{aligned} \Delta\mathbf{B} &= \mathbb{A} : \Delta\mathbf{E} + \mathbb{B} : \Delta\mathbf{K} \\ \Delta\mathbf{G} &= \mathbb{B}^\top : \Delta\mathbf{E} + \mathbb{D} : \Delta\mathbf{K} \end{aligned} \tag{49}$$

Now, we substitute the following Lagrangian interpolation of the kinematic field increments into the increments in Eq. (48):

$$\begin{aligned} \Delta\mathbf{Q} &= \Delta\hat{\varphi}\mathbf{Q} = \hat{\mathbf{I}}\mathbf{Q}\Delta\varphi = \hat{\mathbf{I}}\mathbf{Q}\mathbf{N}_\varphi \Delta\mathbf{d}^\mathbf{e} \\ (\nabla_0 \Delta\mathbf{u})^\top &= (\nabla_0 \mathbf{N}_\mathbf{u})^\top \Delta\mathbf{d}^\mathbf{e} \\ \Delta\mathbf{E} &= \mathbf{Q}^\top (\nabla_0 \mathbf{N}_\mathbf{u} + \hat{\mathbf{I}}^\top \mathbf{F} \mathbf{N}_\varphi) \Delta\mathbf{d}^\mathbf{e} \\ \Delta\mathbf{K} &= \mathbf{Q}^\top \nabla_0 \mathbf{N}_\varphi \Delta\mathbf{d}^\mathbf{e} \end{aligned} \tag{50}$$

then Eq. (48) becomes:

$$\begin{aligned} \Delta\mathrm{f}_i^{\mathbf{e}1} &= (\nabla_0 \mathbf{N}_{\mathbf{u}i})^\top \hat{\mathbf{I}}\mathbf{Q}\mathbf{N}_\varphi \Delta\mathbf{d}^\mathbf{e} : \mathbf{B}^\top + \\ &\quad (\nabla_0 \mathbf{N}_{\mathbf{u}i})^\top \mathbf{Q} : \left(\mathbb{A} : (\mathbf{Q}^\top (\nabla_0 \mathbf{N}_\mathbf{u} + \hat{\mathbf{I}}^\top \mathbf{F} \mathbf{N}_\varphi)) + \mathbb{B} : (\mathbf{Q}^\top \nabla_0 \mathbf{N}_\varphi) \right)^\top \Delta\mathbf{d}^\mathbf{e} \\ \Delta\mathrm{f}_i^{\mathbf{e}2} &= N_{\varphi i} (\nabla_0 \mathbf{N}_\mathbf{u})^\top \Delta\mathbf{d}^\mathbf{e} \hat{\mathbf{I}}\mathbf{Q} : \mathbf{B}^\top + \\ &\quad N_{\varphi i} \mathbf{F}^\top \hat{\mathbf{I}} \hat{\mathbf{I}} \mathbf{Q} \mathbf{N}_\varphi \Delta\mathbf{d}^\mathbf{e} : \mathbf{B}^\top + \\ &\quad N_{\varphi i} \mathbf{F}^\top \hat{\mathbf{I}}\mathbf{Q} : \left(\mathbb{A} : (\mathbf{Q}^\top (\nabla_0 \mathbf{N}_\mathbf{u} + \hat{\mathbf{I}}^\top \mathbf{F} \mathbf{N}_\varphi)) + \mathbb{B} : (\mathbf{Q}^\top \nabla_0 \mathbf{N}_\varphi) \right)^\top \Delta\mathbf{d}^\mathbf{e} \\ \Delta\mathrm{f}_i^{\mathbf{e}3} &= (\nabla_0 N_{\varphi i})^\top \hat{\mathbf{I}}\mathbf{Q}\mathbf{N}_\varphi \Delta\mathbf{d}^\mathbf{e} : \mathbf{G}^\top + \\ &\quad (\nabla_0 N_{\varphi i})^\top \mathbf{Q} : \left(\mathbb{B}^\top : (\mathbf{Q}^\top (\nabla_0 \mathbf{N}_\mathbf{u} + \hat{\mathbf{I}}^\top \mathbf{F} \mathbf{N}_\varphi)) + \mathbb{D} : (\mathbf{Q}^\top \nabla_0 \mathbf{N}_\varphi) \right)^\top \Delta\mathbf{d}^\mathbf{e} \end{aligned} \tag{51}$$

In the Eq. (51), $\Delta\mathbf{d}^\mathbf{e}$ is the basic unknown kinetic increment vector, so we can obtain the element stiffness matrix $\mathbf{K}^\mathbf{e}$ from this equation. Each component of $\mathbf{K}^\mathbf{e}$ can be expressed by considering component form of shape function N_i as:

$$\begin{aligned} (\mathbf{K}^{\mathbf{e}1})_{ij} &= \int_V \Big[(\nabla_0 \mathbf{N}_{\mathbf{u}i})^\top \hat{\mathbf{I}}\mathbf{Q} N_{\varphi j} : \mathbf{B}^\top + \\ &\quad (\nabla_0 \mathbf{N}_{\mathbf{u}i})^\top \mathbf{Q} : \left(\mathbb{A} : (\mathbf{Q}^\top (\nabla_0 \mathbf{N}_{\mathbf{u}j} + \hat{\mathbf{I}}^\top \mathbf{F} N_{\varphi j})) + \mathbb{B} : (\mathbf{Q}^\top \nabla_0 N_{\varphi j}) \right)^\top \Big] \mathrm{d}V \\ (\mathbf{K}^{\mathbf{e}2})_{ij} &= \int_V \Big[N_{\varphi i} (\nabla_0 \mathbf{N}_{\mathbf{u}j})^\top \hat{\mathbf{I}}\mathbf{Q} : \mathbf{B}^\top + \\ &\quad N_{\varphi i} \mathbf{F}^\top \hat{\mathbf{I}} \hat{\mathbf{I}} \mathbf{Q} N_{\varphi j} : \mathbf{B}^\top + \\ &\quad N_{\varphi i} \mathbf{F}^\top \hat{\mathbf{I}}\mathbf{Q} : \left(\mathbb{A} : (\mathbf{Q}^\top (\nabla_0 \mathbf{N}_{\mathbf{u}j} + \hat{\mathbf{I}}^\top \mathbf{F} N_{\varphi j})) + \mathbb{B} : (\mathbf{Q}^\top \nabla_0 N_{\varphi j}) \right)^\top \Big] \mathrm{d}V \\ (\mathbf{K}^{\mathbf{e}3})_{ij} &= \int_V \Big[(\nabla_0 N_{\varphi i})^\top \hat{\mathbf{I}}\mathbf{Q} N_{\varphi j} : \mathbf{G}^\top + \\ &\quad (\nabla_0 N_{\varphi i})^\top \mathbf{Q} : \left(\mathbb{B}^\top : (\mathbf{Q}^\top (\nabla_0 \mathbf{N}_{\mathbf{u}j} + \hat{\mathbf{I}}^\top \mathbf{F} N_{\varphi j})) + \mathbb{D} : (\mathbf{Q}^\top \nabla_0 N_{\varphi j}) \right)^\top \Big] \mathrm{d}V \end{aligned} \tag{52}$$

and,

$$(\mathbf{K}^{\mathbf{e}})_{ij} = (\mathbf{K}^{\mathbf{e1}})_{ij} + (\mathbf{K}^{\mathbf{e2}})_{ij} + (\mathbf{K}^{\mathbf{e3}})_{ij} \tag{53}$$

where $i, j = 1, 2, 3, \ldots, n^e$, n^e is the element total degrees of freedom.

Next, the global stiffness matrix $\mathbf{K}$, incremental displacement vector $\Delta\mathbf{d}$, internal force vector $\mathbf{f}$, and external force vector $\mathbf{r}$ can be obtained by assembling all the element contributions and we can get the standard finite element expression as shown in Eq. (4):

$$\mathbf{K}\Delta\mathbf{d} = \mathbf{r} - \mathbf{f} \tag{54}$$

Once the global displacement vector $\Delta\mathbf{d}$ has been obtained, it can be used to update values of $\mathbf{f}$ and $\mathbf{K}$ for the next iteration procedure. To update $\mathbf{f}$ and $\mathbf{K}$, the following values should be updated. The global incremental translate vector ($\Delta\mathbf{u}$) and microrotation vector ($\Delta\boldsymbol{\varphi}$) can be extracted from $\Delta\mathbf{d}$. Considering the current iteration step is k and iteration step to be updated is $(k+1)$, then,

Updates of global translate and position vectors:

$$\mathbf{u}^{(k+1)} = \mathbf{u}^{(k)} + \Delta\mathbf{u} \tag{55}$$

$$\mathbf{x}^{(k+1)} = \mathbf{x}^{(k)} + \Delta\mathbf{u} \tag{56}$$

Updates of global microrotation vector:

$$\boldsymbol{\varphi}^{(k+1)} = \boldsymbol{\varphi}^{(k)} + \Delta\boldsymbol{\varphi} \tag{57}$$

As in the 2D problem, there is only one microrotation measure. Updates of the microrotation tensor can be described directly by the additive structure of microrotation (Eq. (57)):

$$\mathbf{Q}^{(k+1)} = \begin{bmatrix} \cos(\boldsymbol{\varphi}^{(k+1)}) & -\sin(\boldsymbol{\varphi}^{(k+1)}) \\ \sin(\boldsymbol{\varphi}^{(k+1)}) & \cos(\boldsymbol{\varphi}^{(k+1)}) \end{bmatrix} \tag{58}$$

whereas the general update of microrotation tensor should refer to Eq. (32) as:

$$\mathbf{Q}^{(k+1)} = \mathbf{Q}(\Delta\varphi)\mathbf{Q}(\varphi^{(k)}) \tag{59}$$

Updates of the deformation gradient tensor:

$$\mathbf{F}^{(k+1)} = \nabla_0\mathbf{x}^{(k+1)} = (\nabla_0\mathbf{u}^{(k+1)}) + \mathbf{I} \tag{60}$$

With the values of microrotation tensor $\mathbf{Q}$ and deformation gradient tensor $\mathbf{F}$, the updated Cosserat Lagrangian strain and curvature tensors are evaluated from Eqs. (26) and (27). Finally, the updated Lagrangian stress and couple stress can be obtained from Eq. (30).

In the first iteration, the initial conditions are assumed as:

$$\mathbf{u} = \mathbf{0},\ \mathbf{Q} = \mathbf{I} \tag{61}$$

i.e.

$$\mathbf{F} = \mathbf{I},\ \mathbf{B} = \mathbf{0},\ \mathbf{G} = \mathbf{0} \tag{62}$$

The geometric nonlinear finite element formulations of Cauchy and Cosserat models conducted above are implemented by in–house finite element MATLAB codes which are programmed by the authors based on codes of a linear 2D Cauchy continuum as presented in [55].

3. Numerical simulation

In this section, a planar cantilever beam problem under the plane-stress condition (Fig. 1) is solved by geometric nonlinear Cauchy and Cosserat FEM analysis, where the uniformly distributed load $P/2$ is applied at the top and bottom of the beam with a constant direction. To do so, equilibrium iterations are completed by the Newton–Raphson method for each load step. The energy-convergence criterion is set as $\|\Delta\mathbf{d}(\mathbf{r}-\mathbf{f})\| \leq 10^{-5}$. For comparison, the linear results of these two models will also be presented. One can refer to our previous studies [14,56] for the linear FEM formulation.

As the cantilever beam case was extensively studied in the literature, the reliability of the self-developed geometric nonlinear codes can be validated by comparing the results with those from Refs. [44,57]. In this validation analysis, the beam is considered isotropic and Young's modulus (E) and Poisson's ratio (υ) of the beam are 1.2×10^4 MPa and 0.2. Fig. 2 shows the deflection ratio u_2/L at point A as a function of the load parameter $K = PL^3/(EI)$. It can be seen that the self-developed nonlinear Cauchy code can produce very close results compared with Bath's result [57]. Also, for the Cosserat model with negligible microstructure scale ($l = 10^{-16}$), the result from codes can be validated well by the result from Ramezani et al. [44]. Moreover, in Fig. 2, the behaviors of the Cosserat model with negligible microstructure scale are closer to the behaviors of the Cauchy model, which is consistent with the previous study [35], showing the reliability of the geometric nonlinear Cosserat codes.

The present paper aims to study the geometric nonlinear response of anisotropic Cosserat materials. In order to get the constitutive relations for various anisotropic materials within the Cosserat continuum framework, The above cantilever beam is considered a composite that is made of rigid hexagonal blocks interacting with each other through their material elastic interfaces. Representative geometry of the hexagonal block is shown in Fig. 3 and its detailed descriptions can be found in the early study [58]. Each side of the hexagonal block represents a microstructure. By changing angles $\alpha_1, \alpha_2, \alpha_3$ and side length (l) in Fig. 3, different hexagonal microstructure geometries with various scales can be obtained. In this study, we hypothetically construct three geometries termed regular ($\alpha_1 = 0°, \alpha_2 = \alpha_3 = 30°$), hourglass ($\alpha_1 = 0°, \alpha_2 = \alpha_3 = -20°$) and skew ($\alpha_1 = 0°, -\alpha_2 = \alpha_3 = 30°$), and each of them has three scales, i.e. $s = 1$ ($l = 0.3660$ μm), $s = 0.5$ ($l = 0.1830$ μm), and $s = 0.25$ ($l = 0.0915$ μm).

To study above microstructured composites within the continuum framework, a homogenization procedure [59] was employed to derive the equivalent Cosserat and Cauchy constitutive matrices. With various geometries and scales of microstructures, different anisotropic material properties of the beam can be derived. Here, the homogenization procedure takes 7-blocks representative volume element (RVE) for each of the geometries constructed above, as shown in Fig. 4. Then, the equivalent Cosserat constitutive matrices of above hypothetically constructed microstructured materials can be calculated by considering the constant elastic stiffness assigned to each interface as follows:

$$K = \begin{bmatrix} k_n & 0 \\ 0 & k_t \end{bmatrix} \tag{63}$$

where k_n and k_t are the normal and tangential stiffness, respectively. Here we have $k_n = 576.58$ MPa/μm and $k_t = k_n/2 = 288.29$ MPa/μm. The rotation stiffness of interface is $k_r = k_n(l/2)^2$. Then, the equivalent Cosserat constitutive matrix for each RVE can be obtained by adopting the proposed homogenization method [59].

The calculated constitutive matrix for regular RVEs is:

$$\begin{aligned} \mathbb{A} &= \begin{bmatrix} 1189.7 & 169.96 & 0 & 0 \\ 169.96 & 1189.7 & 0 & 0 \\ 0 & 0 & 849.79 & 169.96 \\ 0 & 0 & 169.96 & 849.79 \end{bmatrix}, \text{MPa} \\ \mathbb{D}^{(s=1)} &= \begin{bmatrix} 108.16 & 0 \\ 0 & 88.234 \end{bmatrix};\ \mathbb{D}^{(s=0.5)} = \begin{bmatrix} 27.039 & 0 \\ 0 & 22.058 \end{bmatrix}; \\ \mathbb{D}^{(s=0.25)} &= \begin{bmatrix} 6.7598 & 0 \\ 0 & 5.5146 \end{bmatrix}, \text{MPa μm}^2 \end{aligned} \tag{64}$$

The calculated constitutive matrix for hourglass RVEs is:

$$\begin{aligned} \mathbb{A} &= \begin{bmatrix} 584.42 & -126.15 & 0 & 0 \\ -126.15 & 2539.9 & 0 & 0 \\ 0 & 0 & 1927.4 & -126.15 \\ 0 & 0 & -126.15 & 346.67 \end{bmatrix}, \text{MPa} \\ \mathbb{D}^{(s=1)} &= \begin{bmatrix} 40.714 & 0 \\ 0 & 196.93 \end{bmatrix};\ \mathbb{D}^{(s=0.5)} = \begin{bmatrix} 10.178 & 0 \\ 0 & 49.233 \end{bmatrix}; \\ \mathbb{D}^{(s=0.25)} &= \begin{bmatrix} 2.5446 & 0 \\ 0 & 12.308 \end{bmatrix}, \text{MPa μm}^2 \end{aligned} \tag{65}$$

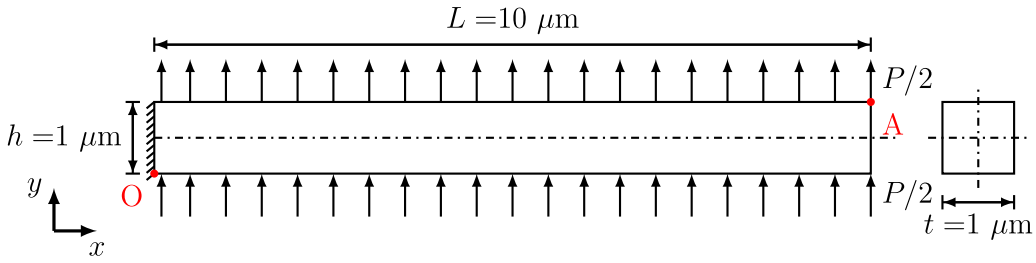

Fig. 1. Sketch of the cantilever beam problem.

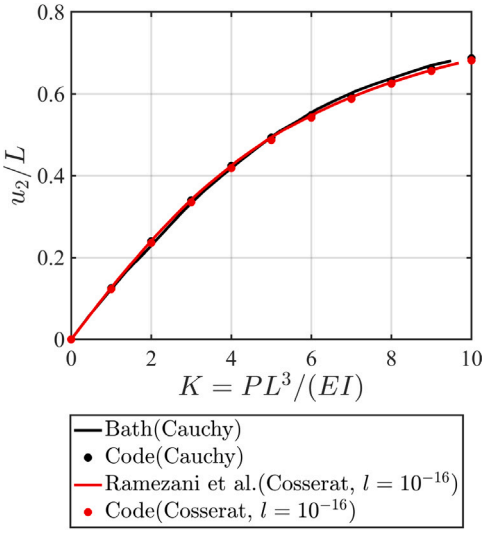

Fig. 2. Nonlinear results obtained from self-developed codes and references.

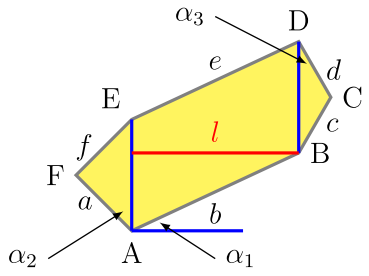

Fig. 3. Representative geometry of hexagonal block.

The calculated constitutive matrix for skew RVEs is:

$$\mathbb{A} = \begin{bmatrix} 793.13 & 0 & 0 & 0 \\ 0 & 1784.6 & 0 & 0 \\ 0 & 0 & 1274.7 & 0 \\ 0 & 0 & 0 & 566.52 \end{bmatrix}, \text{MPa}$$

$$\mathbb{B}^{(s=1)} = \begin{bmatrix} 0 & 0 \\ 0 & 124.42 \\ 0 & 0 \\ 0 & 0 \end{bmatrix}; \quad \mathbb{B}^{(s=0.5)} = \begin{bmatrix} 0 & 0 \\ 0 & 62.209 \\ 0 & 0 \\ 0 & 0 \end{bmatrix};$$

$$\mathbb{B}^{(s=0.25)} = \begin{bmatrix} 0 & 0 \\ 0 & 31.104 \\ 0 & 0 \\ 0 & 0 \end{bmatrix}, \text{MPa μm} \tag{66}$$

$$\mathbb{D}^{(s=1)} = \begin{bmatrix} 65.464 & 0 \\ 0 & 151.56 \end{bmatrix}; \quad \mathbb{D}^{(s=0.5)} = \begin{bmatrix} 16.366 & 0 \\ 0 & 37.891 \end{bmatrix};$$

$$\mathbb{D}^{(s=0.25)} = \begin{bmatrix} 4.0915 & 0 \\ 0 & 9.4727 \end{bmatrix}, \text{MPa μm}^2$$

It can be seen that the constitutive components in $\mathbb{A}$ are not affected by the microstructure's scale, whereas the constitutive components in $\mathbb{B}$ and $\mathbb{D}$ decrease as the scale decreases. Furthermore, the Cauchy constitutive matrices can be obtained from the Cosserat constitutive matrices as [59]:

$$\begin{aligned} \hat{A}_{1111} &= A_{1111} \\ \hat{A}_{1122} &= A_{1122} \\ \hat{A}_{2222} &= A_{2222} \\ \hat{A}_{1112} &= (A_{1112} + A_{1121})/2 \\ \hat{A}_{2212} &= (A_{2212} + A_{2221})/2 \\ \hat{A}_{1212} &= (A_{1212} + A_{2121} + 2A_{1221})/4 \end{aligned} \tag{67}$$

where the symbol $\hat{}$ denotes the Cauchy constitutive components.

4. Results and discussions

Figs. 5–6 show the simulation results of displacements and stresses obtained by nonlinear Cauchy and Cosserat models in the deformed configuration of the cantilever beam. The scale effect of microstructures can be observed for these results. It can be seen that when $s = 1$, there is an apparent difference between the Cosserat result and its Cauchy counterpart. As s decreases, the Cosserat results tend to converge to the Cauchy results. Therefore, the scale effect can be ignored if the microstructure is small enough compared with the macroscopic dimension of the material. However, for materials with larger s, the nonlinear Cauchy model tends to overestimate displacements and stresses that come from nonlinear Cosserat results, implying the significance of the microstructure scale effect.

The cantilever beam with different microstructure geometries has different behaviors under the same load. For the Cauchy model or Cosserat model at the same scale, the hourglass configuration shows the largest horizontal and vertical displacements (u_1 and u_2), while the regular shows the lowest. Thus, it can be seen that the highest deformation of the beam occurs in the hourglass configuration, followed by skew and regular configurations. Table 1 gives values of horizontal (σ_{11}) and vertical stresses (σ_{22}) at point O in Fig. 1. Stress values also show the scale effect as mentioned above. Although the regular microstructure geometry shows the smallest deformation, it has the highest values of σ_{11} and σ_{22}, followed by skew and hourglass configurations. That means that the stress value at point O increases as deformation decreases. Although σ_{22} at point O is much smaller than σ_{11}, one should note that σ_{22} shows different directions for three microstructure geometries. Skew microstructured material has negligible values of σ_{22}. Apart from that, the regular case has positive values of σ_{22}, while the hourglass has negative values. Such differences can be due to different anisotropic material properties produced by these microstructure geometries.

From the deformed shapes shown in Figs. 5–6, it was indicated that the deformation of the cantilever beam is affected by the scales and geometries of microstructures. Fig. 7 further shows the deformed shape of the cantilever beam middle line for nonlinear Cosserat and Cauchy models. Also, the difference between the results of these two models is negligible at small scales. When the scale of microstructures

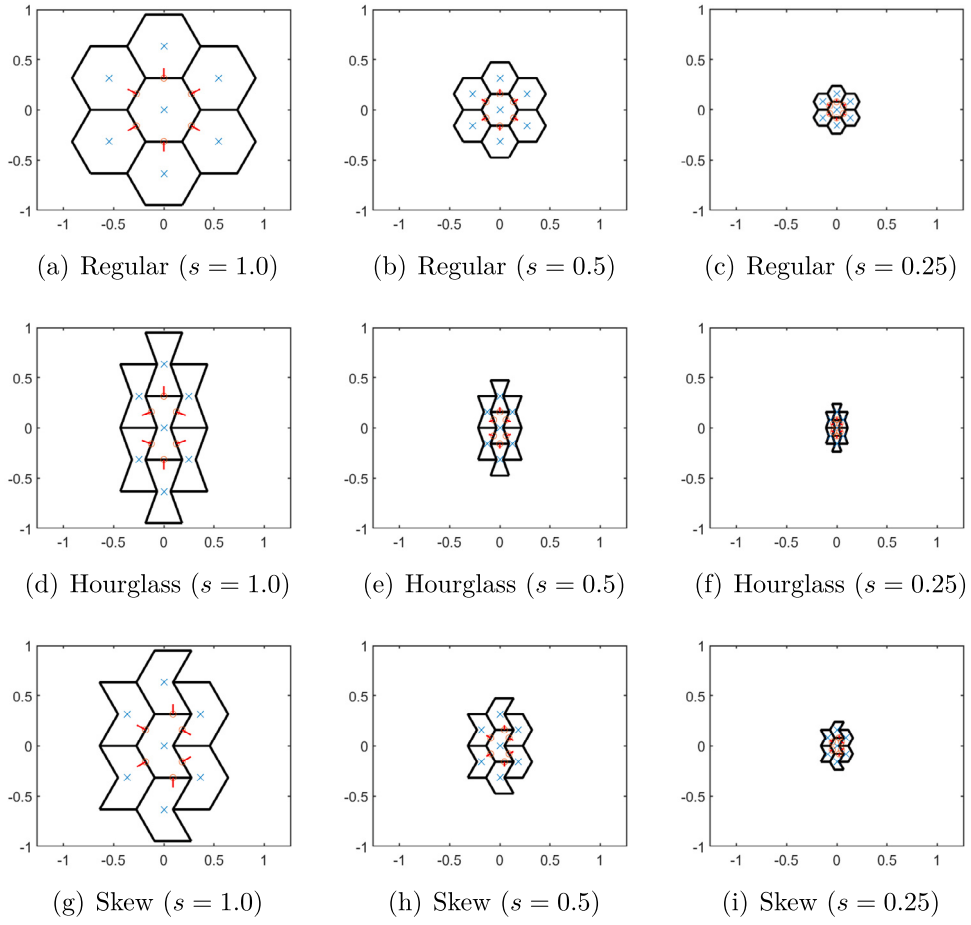

Fig. 4. 7-blocks RVEs with different scale for each kind of hexagonal microstructure.

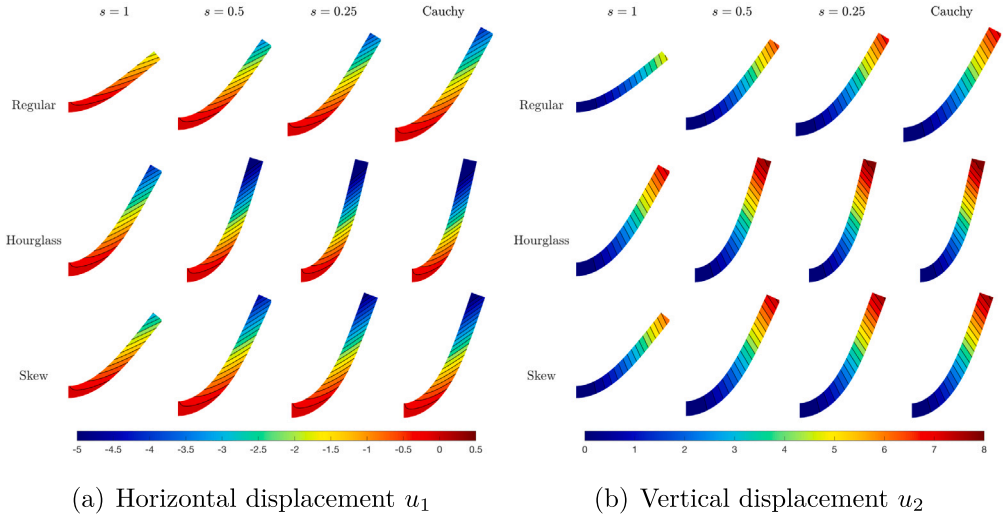

Fig. 5. Displacement fields in the deformed configuration of the cantilever beam, μm.

increases, the deformed curves related to the Cosserat model depart from the curve of the Cauchy model and the deflection of the beam decreases. The microstructure effect in the Cosserat model can be due to the activation of the couple stresses as scale increases, which is able to resist the beam for deflection increases [44]. One can also find in the constitutive matrices (Eqs. (64)–(66)) that as scale increases, $\mathbb{A}$ matrix related to the classical properties of material remains unchanged, whereas the $\mathbb{B}$ and $\mathbb{D}$ matrices related to the microstructure effect increase. That means an increasing scale of microstructures can bring stiffer properties to a material.

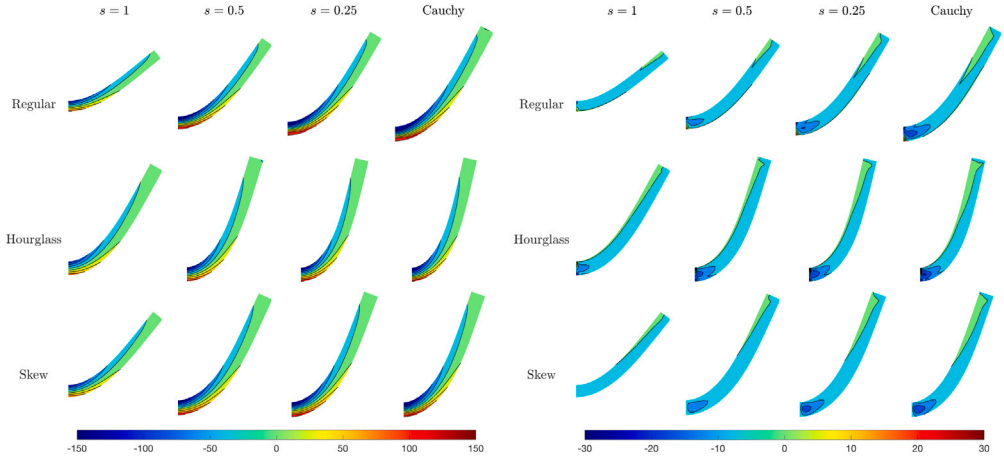

(a) Horizontal stress σ_{11} (b) Vertical stress σ_{22}

Fig. 6. Stress fields in the deformed configuration of the cantilever beam, MPa.

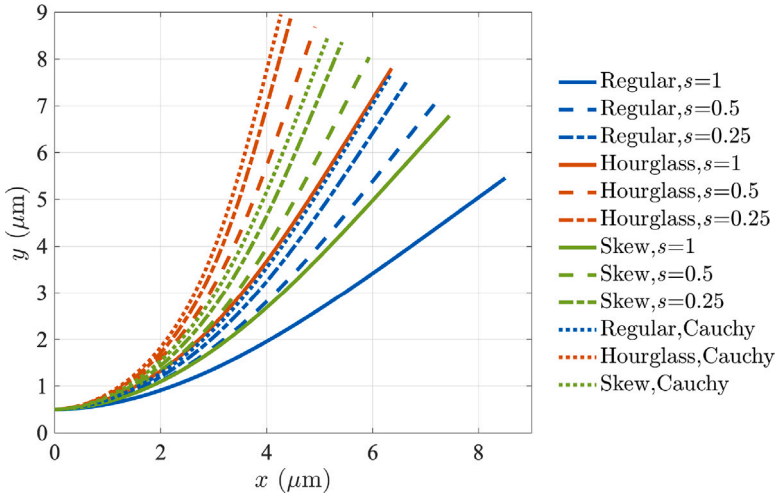

Fig. 7. Deformed shape of the cantilever beam middle line for nonlinear Cosserat and Cauchy models.

Table 1
Stress values at point O, MPa.

		$s = 1$	$s = 0.5$	$s = 0.25$	Cauchy
σ_{11}	Regular	126.86	185.85	213.35	236.12
	Hourglass	114.68	147.47	159.61	173.37
	Skew	119.09	162.82	181.32	198.66
σ_{22}	Regular	17.91	26.07	29.82	32.81
	Hourglass	−26.15	−34.19	−37.27	−41.19
	Skew	−0.59	−1.14	−1.47	−1.96

It is worth mentioning that the linear Cosserat model is also able to demonstrate the microstructure effect. Fig. 8 shows the linear results in the deformed shape of the cantilever beam middle line for two models. However, as it is presented in Figs. 7 and 8, the linear and nonlinear results are quite different. Especially, note that the upper y-axis limit in Fig. 8 is much higher than that in Fig. 7, meaning that linear models can bring more deflection in the vertical direction for the beam. One example comparing the deformed beam shapes of linear and nonlinear models for hourglass microstructures ($s = 1$) is shown in Fig. 9. It can be seen that the results of linear models give impractically greater deformation than nonlinear models, although the scale effect can also be observed. Geometric nonlinear Cauchy and Cosserat models can both give more realistic deformation results. Therefore, for large deformation problems, it is more suitable to use nonlinear models to describe the material's responses.

In Fig. 10, the microrotation along the middle line of the beam is shown on the undeformed configuration. The microrotation represents the rotation of the microstructure that is different from the macrorotation of the body (local rigid rotation). Therefore, it is a peculiar measure in the Cosserat model that can be used to investigate the micropolar effect. It can be seen from Fig. 10 that the increase of microstructure scale also decreases the microrotation for the same microstructure geometry. That also demonstrates that micropolar effects are significant for small microstructures. At the same scale, hourglass microstructures get the most microrotation, while the regular ones get the least. The slope of the microrotation curves is zero at the tip of the beam because there is no external couple stress applied.

Fig. 11 shows variations of deflection versus load at point A for nonlinear models. We can see that there is a nonlinear relationship between load and deflection as we expect. The phenomenon of such nonlinearity is more obvious in the Cauchy model compared with the

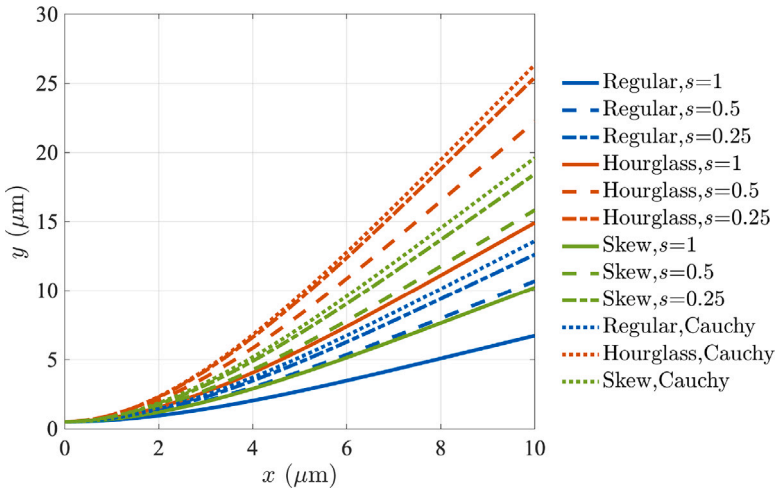

Fig. 8. Deformed shape of the cantilever beam middle line for linear Cosserat and Cauchy models.

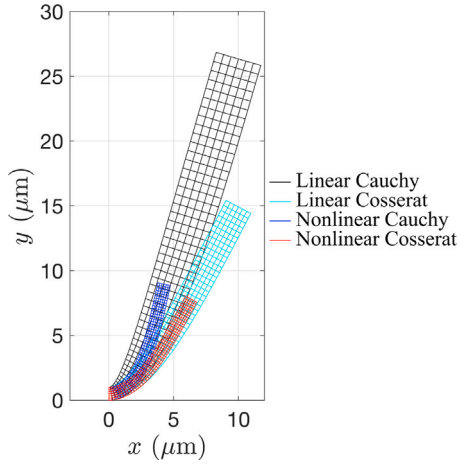

Fig. 9. Comparison of deformed beam shapes between linear and nonlinear models for hourglass microstructure ($s = 1$).

Cosserat model for the same microstructure geometry. In the Cosserat model, the curves with small scales are closer to the Cauchy curve. As the scale increases, the curve departs from the Cauchy result and its degree of nonlinearity gets reduced. For the regular geometry when $s = 1$, the relationship between load and deflection even shows an approximated linear curve. At the same scale, hourglass geometry shows the most evident nonlinear phenomenon, followed by skew and regular. In fact, the nonlinearity between load and deflection becomes obvious as the deformation of the beam increases if we check the above results. That is why we apply the geometric nonlinear study to large deformation problems. The relationship between load and microrotation in the Cosserat model has a similar nonlinear behavior to that between load and deflection, so such results are not shown here.

In this study, taking regular, hourglass, and skew microstructure geometry, different anisotropic materials can be obtained and thus they produce different results by geometric nonlinear models. Reviewing the constitutive matrices of these materials from Eqs. (64)–(66), the regular matrices appeared to be orthotetragonal in which $\mathbb{A}_{1111} = \mathbb{A}_{2222}$, $\mathbb{A}_{1212} = \mathbb{A}_{2121}$, and $\mathbb{D}_{11} = \mathbb{D}_{22}$. No couplings between normal and shear stresses, stresses and curvatures, couple stresses and strains can be observed. These couplings also do not exist in the hourglass material, whereas $\mathbb{A}_{1111} \neq \mathbb{A}_{2222}$, $\mathbb{A}_{1212} \neq \mathbb{A}_{2121}$, and $\mathbb{D}_{11} \neq \mathbb{D}_{22}$ for such material compared with the regular case. Another important characteristic of the hourglass material is the negative Poisson coefficient. This leads to a so-called auxetic behavior of this material. Skew material has no Poisson effect but the couplings between stresses and curvatures, couple stresses and strains appear, ie. $\mathbb{B} \neq 0$. Thus, this material has a chiral behavior. Although these three materials have anisotropic properties, they behave differently because of their specific homogenized characteristics induced by different microstructure arrangements.

Tables 2 and 3 displays the comparison of nonlinear computations between Cauchy and Cosserat models ($s = 0.25$). It can be seen that nonlinear computation can be completed faster with the Cauchy model than with the Cosserat model. Less iteration and time are taken by using the Cauchy model and the computational errors are obviously less than the tolerance (10^{-5}). However, the Cosserat model needs more iterations and time to get the solution in which the computational errors are close to the tolerance. Such a difference can be due to the more extensive computation involved in the Cosserat model. For instance, in the Cosserat model, each stiffness component should be computed individually (see Eq. (52)), whereas in the Cauchy model, the stiffness matrix can be obtained in a whole form. For different microstructured geometries, the hourglass case generally takes the highest cost because of its highest geometric nonlinearity caused by the largest deformation as mentioned above.

5. Conclusions

This work presents the geometrically nonlinear mechanical behavior of anisotropic composite materials with hexagonal microstructures described as equivalent Cosserat continuum. For comparison, results of the nonlinear Cauchy continuum are also presented. Geometric nonlinear implementation is based on the total Lagrangian finite element formulations developed for anisotropic materials that is rarely studied in previous literature. Three equivalent anisotropic materials are obtained by homogenizing a composite consisting of the so-called regular, hourglass, and skew hexagonal microstructure geometries, respectively. Three scales are considered for each type of microstructure geometry. Therefore, the non-locality in the Cosserat continuum involving the scale effect of microstructures on the geometric nonlinear behavior can be investigated.

Numerical study conducted on the classical cantilever beam problem shows that geometric nonlinear Cosserat and Cauchy models are

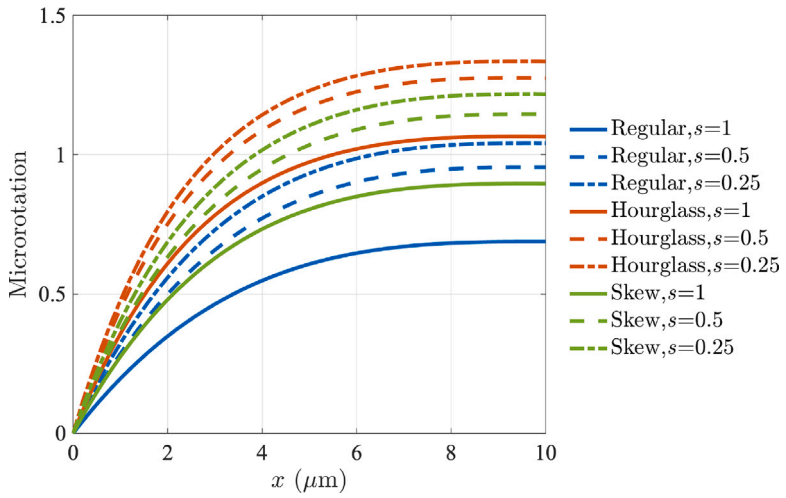

Fig. 10. Microrotation along the cantilever beam middle line for nonlinear Cosserat model.

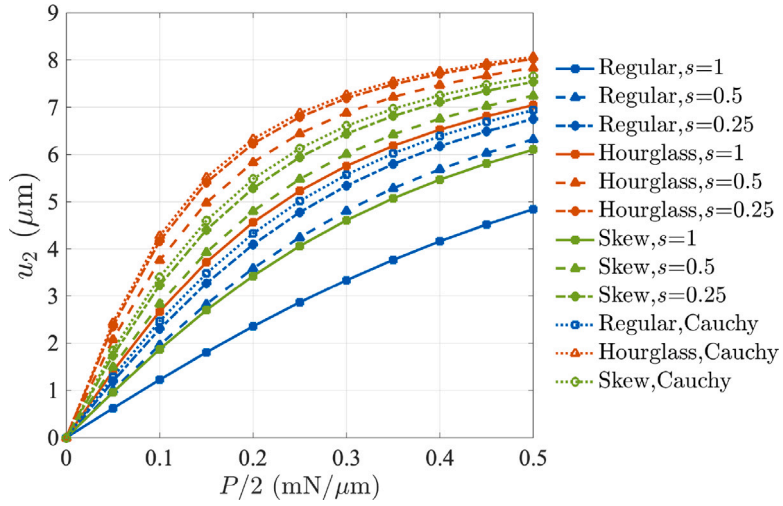

Fig. 11. Load vs. deflection at point A for nonlinear models.

Table 2
Nonlinear computational consumption for Cauchy model.

	Load step	Iterations	Time (s)	Energy error
	1	4	0.3711	3.96E−07
	3	5	0.5012	2.01E−07
Regular	6	5	0.4821	2.69E−09
	8	4	0.3652	9.23E−07
	10	4	0.3709	3.95E−08
	1	5	0.4702	8.52E−07
	3	7	0.6780	8.86E−11
Hourglass	6	5	0.4579	3.32E−07
	8	4	0.3668	1.48E−06
	10	4	0.3648	2.68E−08
	1	5	0.4455	4.32E−10
	3	6	0.5660	4.10E−08
Skew	6	5	0.4595	6.65E−08
	8	4	0.3676	1.43E−06
	10	4	0.3668	3.41E−08

Table 3
Nonlinear computational consumption for Cosserat model (s = 0.25).

	Load step	Iterations	Time (s)	Energy error
	1	4	6.4523	4.67E−07
	3	5	8.0752	5.41E−06
Regular	6	7	11.2690	2.38E−06
	8	7	11.2760	5.15E−06
	10	7	11.2824	7.19E−06
	1	5	8.2032	2.06E−06
	3	7	11.6878	1.50E−06
Hourglass	6	8	13.3121	7.93E−06
	8	9	14.9033	8.32E−06
	10	10	17.0442	6.99E−06
	1	5	8.2180	1.43E−06
	3	6	9.8532	3.85E−06
Skew	6	7	11.4723	9.37E−06
	8	9	14.8609	6.02E−06
	10	10	16.3821	6.95E−06

both able to describe real deformation well, especially for large deformation, compared with linear models showing unreal results if the deformation becomes larger. Moreover, the scale effect can be observed among the Cosseart results. As the scale of microstructure decreases, results obtained by the Cosseart model are closer to those by the Cauchy model. The apparent difference between these two models occurs at a larger microstructure scale, implying that there exists a significant micropolar effect. The nonlinear Cauchy model usually overestimates measures from the Cosserat model, such as stress magnitude, displacement, and hence deformation. Therefore, for the

beam under the same load, the nonlinear Cauchy model and Cosserat model with a small microstructure scale produce larger deformation, implying a more significant effect of scale on the geometric nonlinear behavior when microstructures have smaller scales. The relationship between load and deflection shows varying degrees of nonlinearity according to the deformation. It is found that more deformation can cause a higher degree of nonlinearity, whereas for the small deformation (e.g., deformation occurred for regular microstructures when $s = 1$), load and deflection even show a nearly linear relationship. There are distinct results for different anisotropic materials since each of them has a unique constitutive characteristic. Generally, the hourglass case has the largest deformation and shows the highest degree of nonlinearity result, followed by the skew and regular cases. From the aspect of computation, the nonlinear Cosserat model needs to take more computational effort to obtain a satisfactory solution compared with the Cauchy model, in which the nonlinear computation is faster.

The current work focuses on the theoretical and simulation parts of the geometric nonlinear Cosserat continuum. A limitation of this work can be the lack of practical applications. It is known that the Cosserat continuum has been widely considered in practical applications, such as layered rocks [60], masonry structures [61], and granular materials [62]. For example, in a study [63] of marble rock mechanics, it was found that the marble has microstructures exactly closed to the shape of the regular hexagonal proposed in this paper. Therefore, we believe that the current work can provide a theoretical basis for the practical application of microstructured materials. The authors also plan to combine more actual physical material properties and conduct physical experiments to study practical problems using the nonlinear Cosserat continuum in the future.

CRediT authorship contribution statement

Farui Shi: Writing – review & editing, Writing – original draft, Visualization, Validation, Software, Resources, Methodology, Investigation, Formal analysis, Data curation, Conceptualization. **Nicholas Fantuzzi:** Writing – review & editing, Supervision, Software, Methodology, Funding acquisition, Conceptualization. **Minghui Li:** Supervision, Project administration, Funding acquisition. **Heping Xie:** Supervision, Project administration, Funding acquisition.

Declaration of competing interest

The authors declare that they have no known competing financial interests or personal relationships that could have appeared to influence the work reported in this paper.

Acknowledgments

This work was supported by the China Postdoctoral Science Foundation-CCTEG Joint Support Program under Grant Number 2025T034ZGMK, the Postdoctoral Fellowship Program of CPSF, China under Grant Number GZC20252144, National key research and development program, China (Grant No. 2023YFF0723200), National Natural Science Foundation of China (Nos. 52192625, 52174082 and U22A20166), GuangDong Basic and Applied Basic Research Foundation, China (No. 2025B1515020039), Shenzhen Science and Technology Program, China (No. RCYX20221008092903013), the Program for Guangdong Introducing Innovative and Entrepreneurial Teams, China (2019ZT08G315). Nicholas Fantuzzi acknowledges the support of PRIN 2022, Project 2022YLNJRY (J53D23002500006) which is funded by the European Union - NextGenerationEU.

Data availability

Data will be made available on request.

References

[1] A. Pau, P. Trovalusci, Block masonry as equivalent micropolar continua: the role of relative rotations, Acta Mech. 223 (7) (2012) 1455–1471.
[2] R. Luciano, J. Willis, FE analysis of stress and strain fields in finite random composite bodies, J. Mech. Phys. Solids 53 (7) (2005) 1505–1522.
[3] N. Fleck, G. Muller, M.F. Ashby, J.W. Hutchinson, Strain gradient plasticity: theory and experiment, Acta Met. Mater. 42 (2) (1994) 475–487.
[4] J.S. Stölken, A. Evans, A microbend test method for measuring the plasticity length scale, Acta Mater. 46 (14) (1998) 5109–5115.
[5] M.R. Begley, J.W. Hutchinson, The mechanics of size-dependent indentation, J. Mech. Phys. Solids 46 (10) (1998) 2049–2068.
[6] Q. Ma, D.R. Clarke, Size dependent hardness of silver single crystals, J. Mater. Res. 10 (4) (1995) 853–863.
[7] M.B. Taylor, H. Zbib, M. Khaleel, Damage and size effect during superplastic deformation, Int. J. Plast. 18 (3) (2002) 415–442.
[8] H. Altenbach, T. Sadowski, Failure and Damage Analysis of Advanced Materials, Springer, 2015.
[9] F. Greco, L. Leonetti, R. Luciano, P.N. Blasi, Effects of microfracture and contact induced instabilities on the macroscopic response of finitely deformed elastic composites, Compos. Part B: Eng. 107 (2016) 233–253.
[10] P. Trovalusci, M. Ostoja-Starzewski, Multiscale mechanical modelling of complex materials and engineering applications 2, Int. J. Multiscale Comput. Eng. 9 (5) (2011).
[11] N. Fantuzzi, New insights into the strong formulation finite element method for solving elastostatic and elastodynamic problems, Curved Layer. Struct. 1 (1) (2014).
[12] A. Bacigalupo, L. Gambarotta, Dispersive wave propagation in two-dimensional rigid periodic blocky materials with elastic interfaces, J. Mech. Phys. Solids 102 (2017) 165–186.
[13] H. Altenbach, V.A. Eremeyev, Generalized Continua-From the Theory to Engineering Applications, vol. 541, Springer, 2012.
[14] N. Fantuzzi, P. Trovalusci, R. Luciano, Material symmetries in homogenized hexagonal-shaped composites as cosserat continua, Symmetry 12 (3) (2020) 441.
[15] A.C. Eringen, Theory of micropolar elasticity, in: Microcontinuum Field Theories, Springer, 1999, pp. 101–248.
[16] E. Cosserat, F. Cosserat, Theorie des Corps Dédormables, A. Hermann et fils, 1909.
[17] A.C. Eringen, Linear theory of micropolar elasticity, J. Math. Mech. (1966) 909–923.
[18] C. Kafadar, A.C. Eringen, Micropolar media–I the classical theory, Internat. J. Engrg. Sci. 9 (3) (1971) 271–305.
[19] D. Addessi, E. Sacco, Cauchy and cosserat equivalent continua for the multiscale analysis of periodic masonry walls, Trends Comput. Contact Mech. (2011) 253–268.
[20] J. Jeong, H. Ramézani, F. Benboudjema, Numerical Implementation of the Deformation of Drying Shrinkage of the Cement-based Materials: Effect of Micro structure-Cauchy's Approach or Second Gradient Approach, vol. 2009, European Comsol Conference in Milan, Italy, 2009.
[21] J. Jeong, P. Mounanga, H. Ramézani, M. Bouasker, A new multi-scale modeling approach based on hygro-Cosserat theory for self-induced stress in hydrating cementitious mortars, Comput. Mater. Sci. 50 (7) (2011) 2063–2074.
[22] A.J. Beveridge, M. Wheel, D. Nash, A higher order control volume based finite element method to predict the deformation of heterogeneous materials, Comput. Struct. 129 (2013) 54–62.
[23] S. Grbčić, A. Ibrahimbegović, G. Jelenić, Variational formulation of micropolar elasticity using 3D hexahedral finite-element interpolation with incompatible modes, Comput. Struct. 205 (2018) 1–14.
[24] S. Grbčić, G. Jelenić, D. Ribarić, Quadrilateral 2D linked-interpolation finite elements for micropolar continuum, Acta Mech. Sin. 35 (5) (2019) 1001–1020.
[25] L. Li, S. Xie, Finite element method for linear micropolar elasticity and numerical study of some scale effects phenomena in MEMS, Int. J. Mech. Sci. 46 (11) (2004) 1571–1587.
[26] P. Trovalusci, R. Masiani, A multifield model for blocky materials based on multiscale description, Int. J. Solids Struct. 42 (21–22) (2005) 5778–5794.
[27] X. Li, Q. Liu, J. Zhang, A micro–macro homogenization approach for discrete particle assembly–Cosserat continuum modeling of granular materials, Int. J. Solids Struct. 47 (2) (2010) 291–303.
[28] H.-B. Mühlhaus, Continuum models for layered and blocky rock, in: Analysis and Design Methods, Elsevier, 1993, pp. 209–230.
[29] S. Forest, K. Sab, Cosserat overall modeling of heterogeneous materials, Mech. Res. Commun. 25 (4) (1998) 449–454.
[30] E. Pasternak, A.V. Dyskin, On a possibility of reconstruction of cosserat moduli in particulate materials using long waves, Acta Mech. 225 (8) (2014) 2409–2422.
[31] J. Sulem, I. Stefanou, E. Veveakis, Stability analysis of undrained adiabatic shearing of a rock layer with Cosserat microstructure, Granul. Matter 13 (3) (2011) 261–268.
[32] J. Žalohar, On a new law of faulting along tectonic wedges: Cosserat explanation of the preferred (paleo) stress states in the Earth's crust, J. Struct. Geol. 77 (2015) 107–125.

[33] A.C. Eringen, Theory of micropolar fluids, J. Math. Mech. (1966) 1–18.
[34] A. Bhattacharyya, B. Mukhopadhyay, Study of linear isotropic micro-polar plate in an asymptotic approach, Comput. Math. Appl. 66 (6) (2013) 1047–1057.
[35] L. Leonetti, N. Fantuzzi, P. Trovalusci, F. Tornabene, Scale effects in orthotropic composite assemblies as micropolar continua: A comparison between weak-and strong-form finite element solutions, Materials 12 (5) (2019) 758.
[36] C. Sansour, S. Skatulla, A non-linear cosserat continuum-based formulation and moving least square approximations in computations of size-scale effects in elasticity, Comput. Mater. Sci. 41 (4) (2008) 589–601.
[37] W. Pietraszkiewicz, V. Eremeyev, On natural strain measures of the non-linear micropolar continuum, Int. J. Solids Struct. 46 (3–4) (2009) 774–787.
[38] W. Pietraszkiewicz, V. Eremeyev, On vectorially parameterized natural strain measures of the non-linear Cosserat continuum, Int. J. Solids Struct. 46 (11–12) (2009) 2477–2480.
[39] V.A. Eremeyev, W. Pietraszkiewicz, Material symmetry group of the non-linear polar-elastic continuum, Int. J. Solids Struct. 49 (14) (2012) 1993–2005.
[40] V.A. Eremeyev, W. Pietraszkiewicz, Material symmetry group and constitutive equations of micropolar anisotropic elastic solids, Math. Mech. Solids 21 (2) (2016) 210–221.
[41] S. Bauer, M. Schäfer, P. Grammenoudis, C. Tsakmakis, Three-dimensional finite elements for large deformation micropolar elasticity, Comput. Methods Appl. Mech. Engrg. 199 (41–44) (2010) 2643–2654.
[42] S.G. Erdelj, G. Jelenić, A. Ibrahimbegović, Geometrically non-linear 3D finite-element analysis of micropolar continuum, Int. J. Solids Struct. 202 (2020) 745–764.
[43] A. Misra, L. Placidi, E. Barchiesi, et al., Identification of a geometrically nonlinear micromorphic continuum via granular micromechanics, Z. Angew. Math. Phys. 72 (4) (2021) 1–21.
[44] S. Ramezani, R. Naghdabadi, S. Sohrabpour, Non-linear finite element implementation of micropolar hypo-elastic materials, Comput. Methods Appl. Mech. Engrg. 197 (49–50) (2008) 4149–4159.
[45] H. Ramézani, A. El-Hraiech, J. Jeong, C.-L. Benhamou, Size effect method application for modeling of human cancellous bone using geometrically exact cosserat elasticity, Comput. Methods Appl. Mech. Engrg. 237 (2012) 227–243.
[46] P. Steinmann, A micropolar theory of finite deformation and finite rotation multiplicative elastoplasticity, Int. J. Solids Struct. 31 (8) (1994) 1063–1084.
[47] C. Sansour, H. Bufler, An exact finite rotation shell theory, its mixed variational formulation and its finite element implementation, Internat. J. Numer. Methods Engrg. 34 (1) (1992) 73–115.
[48] C. Sansour, H. Bednarczyk, The cosserat surface as a shell model, theory and finite-element formulation, Comput. Methods Appl. Mech. Engrg. 120 (1–2) (1995) 1–32.
[49] E. Providas, M. Kattis, Finite element method in plane Cosserat elasticity, Comput. Struct. 80 (27–30) (2002) 2059–2069.
[50] N. Fantuzzi, P. Trovalusci, S. Dharasura, Mechanical behavior of anisotropic composite materials as micropolar continua, Front. Mater. 6 (2019) 59.
[51] S. Grbčić, Linked interpolation and strain invariance in finite-element modelling of micropolar continuum (Ph.D. thesis), University of Rijeka. Faculty of Civil Engineering, Rijeka, 2018.
[52] K.-J. Bathe, Finite Element Procedures, Klaus-Jurgen Bathe, 2006.
[53] J.N. Reddy, An Introduction to Nonlinear Finite Element Analysis Second Edition: with applications to heat transfer, fluid mechanics, and solid mechanics, OUP Oxford, 2014.
[54] J. Jeong, H. Ramézani, Enhanced numerical study of infinitesimal non-linear Cosserat theory based on the grain size length scale assumption, Comput. Methods Appl. Mech. Engrg. 199 (45–48) (2010) 2892–2902.
[55] A.J. Ferreira, N. Fantuzzi, MATLAB codes for finite element analysis: Solids and Structures, second ed. Springer, 2020.
[56] F. Shi, N. Fantuzzi, P. Trovalusci, Y. Li, Z. Wei, The effects of dilatancy in composite assemblies as micropolar continua, Compos. Struct. 276 (2021) 114500.
[57] K.-J. Bathe, E. Ramm, E.L. Wilson, Finite element formulations for large deformation dynamic analysis, Internat. J. Numer. Methods Engrg. 9 (2) (1975) 353–386.
[58] N. Fantuzzi, P. Trovalusci, R. Luciano, Multiscale analysis of anisotropic materials with hexagonal microstructure as micropolar continua, Int. J. Multiscale Comput. Eng. 18 (2) (2020).
[59] P. Trovalusci, R. Masiani, Material symmetries of micropolar continua equivalent to lattices, Int. J. Solids Struct. 36 (14) (1999) 2091–2108.
[60] D. Bigoni, P.A. Gourgiotis, Folding and faulting of an elastic continuum, Proc. R. Soc. A: Math. Phys. Eng. Sci. 472 (2187) (2016) 20160018.
[61] M. Godio, I. Stefanou, K. Sab, J. Sulem, Cosserat elastoplastic finite elements for masonry structures, Key Eng. Mater. 624 (2014) 131–138.
[62] X. Li, Y. Liang, Q. Duan, B. Schrefler, Y. Du, A mixed finite element procedure of gradient cosserat continuum for second-order computational homogenisation of granular materials, Comput. Mech. 54 (5) (2014) 1331–1356.
[63] F. Bu, J. Peng, L. Wang, B. Dai, J. Zhu, X. Wu, Influence of different cooling treatments on micro-cracking behaviour of marble: Insight from grain-based modelling, Comput. Geotech. 191 (2026) 107773.